SAND2022-7034C

Analyzing Hosting Capacity Protection Constraints Under Time-Varying PV Inverter Fault Response

Joseph A. Azzolini, Nicholas S. Gurule, Rachid Darbali-Zamora, and Matthew J. Reno

Sandia National Laboratories, Albuquerque, NM, 87123, USA

***Abstract*—The proper coordination of power system protective devices is essential for maintaining grid safety and reliability but requires precise knowledge of fault current contributions from generators like solar photovoltaic (PV) systems. PV inverter fault response is known to change with atmospheric conditions, grid conditions, and inverter control settings, but this time-varying behavior may not be fully captured by conventional static fault studies that are used to evaluate protection constraints in PV hosting capacity analyses. To address this knowledge gap, hosting capacity protection constraints were evaluated on a simplified test circuit using both a time-series fault analysis and a conventional static fault study approach. A PV fault contribution model was developed and utilized in the test circuit after being validated by hardware experiments under various irradiances, fault voltages, and advanced inverter control settings. While the results were comparable for certain protection constraints, the time-series fault study identified additional impacts that would not have been captured with the conventional static approach. Overall, while conducting full time-series fault studies may become prohibitively burdensome, these findings indicate that existing fault study practices may be improved by including additional test scenarios to better capture the time-varying impacts of PV on hosting capacity protection constraints.**

***Keywords*—advanced inverters, fault analysis, hosting capacity analysis, power system protection, time-series analysis**

I. Introduction

Before a new solar photovoltaic (PV) system installation is allowed to connect to the power grid, a number of screens and analysis tools are often applied to ensure the safety and reliability of the integrated system. PV hosting capacity analysis (HCA) is one tool that can be used to determine the maximum allowable amount of PV that can be installed on a feeder or at a given location on the grid before certain operating constraints are violated [1], such as exceeding thermal loading limits on power lines or transformers [2], inducing extreme voltages beyond acceptable ranges [3], or causing the miscoordination of protective devices [4]. Like many other types of grid-impact studies, there has been growing interest in evaluating PV hosting capacity as a time-series to better capture the time-varying and time-dependent aspects of both the grid and the PV systems [5]. However, when it comes to evaluating protection constraints for HCA, conventional static fault studies are used that typically only consider when the PV system is operating at unity power factor (PF) and full output capacity. Since the fault contribution of a PV system depends on several time-varying parameters [6], static fault studies may not be sufficient to capture the full range of PV impacts on protection.

Over time, PV inverter capabilities and design topologies have evolved in response to technological advances and updated interconnection standards [7], which has influenced their behavior during blue-sky conditions as well as their response to fault conditions. PV inverters must be able to ride through a variety of disturbances to voltage, frequency, and phase angle [8], and their response to those disturbances depends on whether they are grid-following or grid-forming inverters [9]. Advanced capabilities also enable PV inverters to provide grid support through autonomous control objectives like Volt-VAR or Volt-WATT, as well as to participate in feeder wide control schemes like conservation voltage reduction (CVR), Volt/VAR optimization (VVO), or other specialized objectives of distributed energy resource management systems (DERMS) [10]. Through these advanced control objectives, PV systems may be required to operate over a wide range of non-unity PFs and/or curtail real power based on time-varying atmospheric or grid conditions. While these control objectives and operating conditions do impact PV inverter fault response, HCA tools rely on a conventional static fault analysis method that typically only considers a small set of PV operating conditions like constant unity PF and pre-fault PV output at zero or full capacity.

Many studies have investigated the impacts of distributed PV on protection systems [11], but the degree to which existing HCA fault study assumptions and practices are suitable to evaluate modern PV inverter impacts remains unclear. This paper explores this knowledge gap by first applying hardware tests to validate a PV inverter fault model, then evaluating protection constraints on a test circuit using both conventional static fault analysis and a time-series fault analysis approach. Specifically, this paper combines yearlong time-series power flow simulations with corresponding fault studies at each time point to evaluate the PV impact on two common HCA protection constraints. The main contributions of this paper include:

- A hardware-validated PV fault contribution model that is applicable for different irradiances, fault voltages, and inverter Volt-VAR functions
- A time-series fault analysis methodology
- A static vs. time-series fault analysis comparison and recommendations to improve existing practices

This material is based upon work supported by the U.S. Department of Energy's Office of Energy Efficiency and Renewable Energy (EERE) under the Solar Energy Technologies Office (SETO). Sandia National Laboratories is a multimission laboratory managed and operated by National Technology and Engineering Solutions of Sandia, LLC., a wholly owned subsidiary of Honeywell International, Inc., for the U.S. Department of Energy's National Nuclear Security Administration under contract DE-NA0003525.

Overall, this paper highlights the importance of inverter modeling and time-series analysis for achieving accurate PV HCA results and ensuring a safe and reliable electric grid.

II. Background

The protection system is designed to rapidly isolate and remove faults on the grid as they occur while minimizing the disconnection of customers. Before PV systems and other distributed energy resources (DERs) were present on the grid, protection systems were designed to recognize and respond to large fault currents flowing from the substation to the fault location. When DERs are installed, they can lead to reverse power flows and fault currents from multiple injection points that either increase or decrease fault currents "seen" by protective devices, meaning the "legacy" protection systems may no longer be able to detect certain faults or may inadvertently disconnect more customers than necessary [12, 13]. Specifically, the scenarios of interest in this work are when faults occur downstream of the PV system where the voltage remains high enough at the PV location that the PV system continues to inject current, or "ride through" the low voltage event. If the fault occurs between the PV system and the substation, the PV will stop injecting current (i.e., it will have no impact on the protection system).

To avoid these types of issues, PV planning and interconnection studies often include static fault studies to evaluate existing protection systems for potential impacts [14], like relay desensitization, loss of coordination, nuisance tripping, sympathetic tripping, etc. The fault studies analyze a variety of fault types (e.g., single-line-to-ground, line-to-line, etc.) at different grid locations and with different resistances. PV systems are typically represented by simplified short-circuit models in which the PV system is modeled as a fixed current source outputting 1.2x its per unit (p.u.) rated current in phase with the voltage (i.e., a grid-following PV inverter operating at unity PF). Protection studies will then coordinate settings for protective devices considering the fault study results for this full-rated PV output contribution and the case of zero PV output (i.e., when a fault occurs during the nighttime when PV is off).

These conventional assumptions used in static fault studies for PV inverter fault response may not always be applicable. First, PV inverters only operate at full output capacity for a fraction of the year. PV output changes throughout the day and seasonally as irradiance and temperature change. Second, the PV inverter fault current is not always in phase with the voltage. Today, PV inverters must be capable of responding to centralized control signals from grid operators and be able to operate in a variety of autonomous grid-support modes [7], meaning an inverter may operate at a wide range of PFs and maintain those PFs during faults [6]. Lastly, PV inverter current limits are not standardized, meaning the 1.2x assumption could be an over- or under-estimation of an inverter's actual output current limit; furthermore, some PV inverters apply their current limit based on pre-fault output current (e.g., about 1.1x in [15]), and unlike synchronous generators, inverter fault response can vary from one manufacturer to another [16]. Novel protection schemes are being developed to accommodate these behaviors and characteristics, but their success is dependent upon the accuracy of the underlying inverter models [17].

III. Steady-State PV Inverter Fault Model

This work is focused on the impacts of steady-state fault current injections from PV inverters. In general, when a fault occurs on a circuit, the voltage will sag at the output terminals of the PV inverter, or its point of common coupling (PCC), based on the characteristics and proximity of the fault. Initially, a transient current spike is observed that lasts for about 0.1 ms, meaning the energy contained in the spike is small enough to be ignored by protection schemes [18]. The inverter fault current will then settle to its steady-state value, which is proportional to the fault voltage and subject to the internal current limiting characteristics of the inverter. As noted earlier, some inverters do limit their fault current based on pre-fault output current [15]. However, with all else equal, applying a current limit based on the output current rating of an inverter would result in higher fault current magnitudes and would therefore be of more interest from the perspective of protection system impacts.

A. Model Definition

From here on, the phrase "fault current injection" will refer to the magnitude and angle of the steady-state PV inverter positive-sequence current output during a fault, I_F, defined in (1) as:

$$I_F = |I_F| \angle \Theta_I \tag{1}$$

where $|I_F|$ represents the fault positive-sequence current magnitude and Θ_I represents the angle difference between positive-sequence current and positive-sequence voltage. For this paper, it is assumed that PV inverters are grid-following type inverters that do not inject any negative sequence current [19], so all quantities and variables are positive-sequence values from here on. The fault current magnitude is subsequently defined in (2):

$$|I_F| = \left| \left(\frac{P_{Pre}/PF}{V_F} \right) \right| \tag{2}$$

where P_{Pre} is the pre-fault real power output of the inverter, PF is the pre-fault PF, V_F is the PCC fault voltage, and that (2) is subject to the following constraints:

$$|I_F| \leq I_{Limit} \tag{3}$$
$$\max(S_{Pre}) \leq S_{Rated} \tag{4}$$
$$S_F \leq S_{Pre} \tag{5}$$
$$PF_F = PF_{Pre} = PF \tag{6}$$
$$|I_F| = 0, when\ V_F < 0.5\ p.u. \tag{7}$$

Constraint (3) states that the output current magnitude is bound by the current limit of the inverter, I_{Limit}, which is expressed as a p.u. factor of its output current rating. Constraints (4) and (5) describe that apparent power output cannot exceed the apparent power rating of the inverter (expressed in kVA or p.u.), and that the pre-fault output, S_{Pre}, will be maintained during the fault, S_F, unless the current magnitude was limited. Regardless of whether the fault current is limited, the pre-fault PF, PF_{Pre}, will be maintained during the fault [6], PF_F, and can simply be referred to as PF as in (6). One exception to this constraint is if the inverter is set to provide dynamic voltage support; in this case, the inverter would output reactive power to support the voltage during a fault regardless of the pre-fault PF [7] but analysis of this capability is beyond the scope of this work. Lastly, constraint (7) represents the momentary cessation requirement

from [7], in which the PV inverter shall cease to inject current if the fault voltage, V_F, at its PCC falls below 0.5 p.u. (meaning $|I_F|$ is zero when V_F is less than 0.5 p.u.).

The injection angle of the PV inverter fault current is defined in (8). Since Constraint (6) also applies to (8), Θ_I will be maintained during the fault as well.

$$\Theta_I = \cos^{-1}(PF) \tag{8}$$

Each of the dependent variables of I_F may vary through time; P_{Pre} depends on the PV array output which changes with irradiance and temperature, V_F changes with fault characteristics, and PF changes based on the control objective for the PV system. For example, when the inverter is set to operate in autonomous Volt-VAR mode per [7], PF will change based on P_{Pre} and pre-fault PCC voltage.

B. Model Validation and Current Limit Calibration

The steady-state PV inverter fault model defined in Section III. A. was validated through hardware testing of an actual 3-phase 33 kVA PV inverter using the test setup depicted in Fig. 1. The input terminals of the inverter were connected to a PV array simulator and the output terminals were connected to a grid simulator. For all hardware tests, the simulated PV array size was set to 33 kW (i.e., a DC/AC ratio of 1) such that the value of irradiance (in kW/m^2) would be equivalent to P_{Pre} in p.u., and the simulated temperature was held constant at 25°C. Overall, this setup enabled each of the time-varying parameters of I_F to be controlled independently.

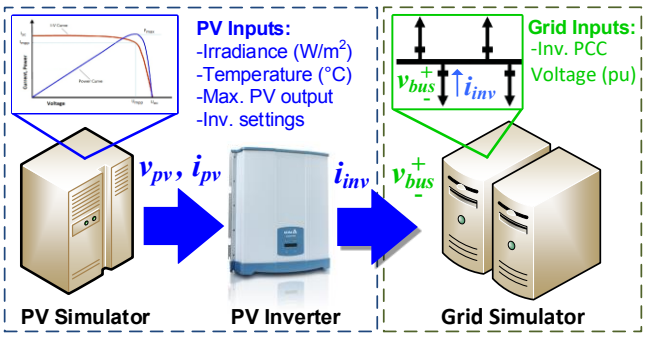

Fig. 1. Experimental setup for PV inverter hardware testing.

The first set of tests was designed to validate the relationship between PV inverter fault current magnitude and fault voltage. For these tests, the inverter was set to operate at unity PF (PF=1), and irradiance was held constant (at 0.9 and 0.2 kW/m^2) while different fault voltages were applied. During the first voltage sweep with irradiance at 0.9 kW/m^2, it was observed that the inverter when into momentary cessation when the fault voltage was below 0.5 p.u. as required by [7] and that the output current was limited at 1.625x the nominal current rating of the inverter (i.e., 1.625 p.u.), much higher than conventional assumptions that are around 1.1-1.2 p.u., as observed in [18].

Based on these results, the default inverter model in OpenDSS [20] was modified in several ways to accommodate the 1.625 p.u. current limit and to ensure it was applied according to equations (1) through (8). By default, the current limit in OpenDSS is determined by the reciprocal of the *Vminpu* parameter. This default model does agree with electromagnetic transient (EMT) inverter models under full PV output and relatively high fault voltages [17] but since the current limit is applied as a function of pre-fault output current, it does not hold under low irradiance and low fault voltage conditions for inverters that limit current as a function of their rated current. Therefore, the proposed model was implemented by dynamically adjusting *Vminpu* as PV and grid conditions changed; specifically, *Vminpu* was kept near zero unless the positive sequence fault current was above 1.625 p.u.

After the inverter model was calibrated, the hardware test setup was replicated in simulation (i.e., connecting a voltage source directly to the PCC terminals of the inverter model and manually adjusting the PV array inputs). The hardware and simulation results are presented in Fig. 2, which shows that, aside from a slight difference in losses, the inverter model sufficiently captures the relationship between fault current magnitude and fault voltage. Since the PV system had a DC/AC ratio of 1 and operated at unity PF, irradiance was equal to the product of voltage and current for any data points that were not current-limited (i.e., apparent power balance was maintained). For illustrative purposes, the momentary cessation feature was not included in the simulation results, and the voltage sweep was repeated after setting the PV array irradiance to 0.5 kW/m^2.

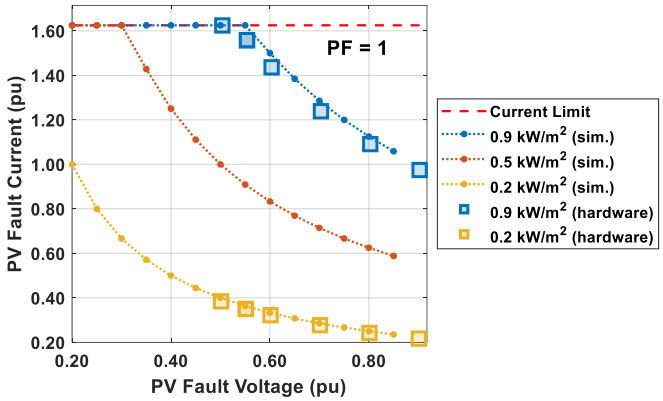

Fig. 2. Inverter fault current magnitude vs. fault voltage (V_F) at unity PF.

The next set of tests was conducted to validate the relationship between fault current magnitude and pre-fault real power output of the inverter, which is directly proportional to irradiance in this case since the DC/AC ratio was set to 1 and temperature was held constant. The inverter was set to unity PF and a fault voltage of 0.55 p.u. was applied after adjusting the input irradiance to various levels. This test was then replicated in simulation, and repeated for fault voltages of 0.45 p.u. and 0.65 p.u. The results are presented in Fig. 3, which show that the inverter model matched the hardware results and the current limit of 1.625 p.u. was once again visible. When voltage and PF were held constant, the linear relationship between fault current and irradiance was observed, as predicted by (2).

The last set of tests investigated the relationship between fault current magnitude and PF. The results are presented in Fig. 4, where the tick marks on the x-axis are spaced according to Θ_I (in degrees). The fault conditions, in this case, included a voltage sag to 0.80 p.u. and a -20° change in positive sequence voltage phase angle, which is within the ride-through requirements [7] and matches values used in prior work [6] that were based on

fault simulations on an actual 21.7 km-long distribution feeder model. According to Equation (2) and Constraint (4), the maximum possible fault current magnitude for a fault voltage of 0.80 p.u. is 1.25 p.u., as confirmed by the simulation and hardware results in Fig. 4. This figure shows that when real power is held constant, the fault current magnitude increases with the reactive power associated with the non-unity PFs until the current limit is reached. At this point, the current magnitude remains constant, but the current angle continues to change. The inverter was also able to quickly synchronize to the step-change in phase angle and operate at a very wide range of PFs, even under low irradiance conditions (0.05 kW/m^2), meaning it is able to operate at practically any PF required by autonomous or centralized controls.

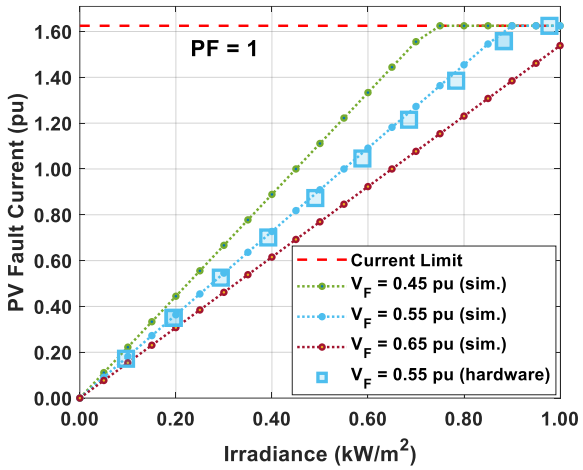

Fig. 3. Inverter fault current magnitude vs. irradiance (i.e., P_{Pre}) at unity PF.

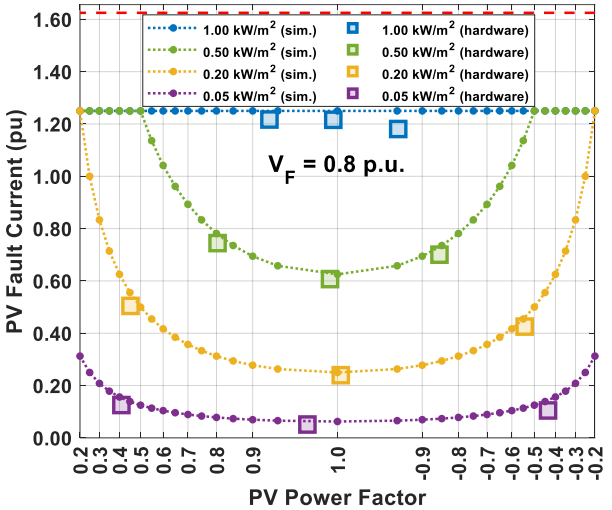

Fig. 4. Inverter fault current magnitude vs. PF (V_F = 0.8 p.u.).

While other inverters may have stricter limitations that are more aligned with the minimum requirements in IEEE 1547 [7], the capabilities depicted in Fig. 4 would still represent the more interesting case in terms of protection system impacts since it essentially has the widest possible operating range of P_{Pre} and *PF*; also, IEEE Std P2800-2022 recommends that large-scale PV inverters be able to meet minimum reactive power capabilities at all active power output levels (including at zero) [21], so it is conceivable that future iterations of distribution interconnection standards might follow similar trends.

IV. Methods

The remainder of the paper analyzes the differences between conventional static fault studies and time-series fault studies for evaluating protection system impacts associated with PV HCA. The following subsections describe the test circuit, introduce the protection system impact metrics evaluated, and present the methodologies for the static and time-series fault studies.

A. Test Circuit

The test circuit depicted in Fig. 5 was created to showcase some of the potential impacts of PV on protection devices and how those impacts vary throughout time as the PV output and grid conditions change. Note that the PV system was placed near the substation so that the voltage it experiences during a fault would be high enough for the PV inverter to ride through (i.e., >0.5 p.u.). Also, the closer the PV is to the substation, the greater the potential there is for desensitization of substation relays to occur.

The circuit was modeled in OpenDSS [20] and represents a 5 km long distribution feeder that contains two protective devices (a substation relay and a recloser), an aggregated load at the end of the feeder, and a large PV system with a grid-following inverter connected through a step-up transformer located 1 km downstream of the substation. The feeder is supplied by a voltage source that represents the sub-transmission system and the voltage on the feeder is regulated by a load-tap changer (LTC) on the substation transformer. The fault location (between the recloser and load, as shown in Fig. 5) and characteristics (a 3-line-to-ground, or 3LG, fault with 1-ohm resistance) were held constant for all static and time-series fault studies. This work focuses on 3LG faults since single-line-to-ground faults are generally detected by the ground overcurrent elements. The 3LG faults are the most extreme fault currents seen, and are the most susceptible to any desensitization or impacts due to the balanced PV current injections.

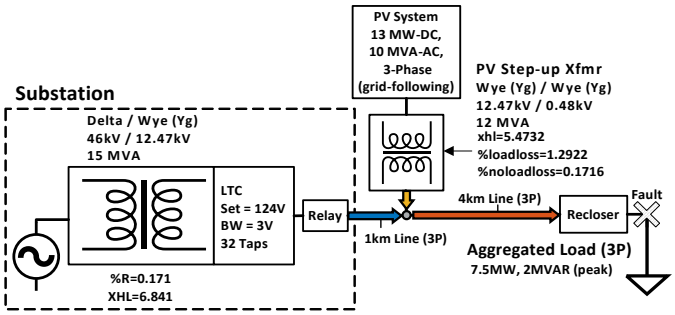

Fig. 5. Diagram of test circuit used for static and time-series fault studies.

To accommodate the time-series simulations, each of the time-varying elements in the circuit was assigned yearlong profiles with 15-minute resolutions that dictate the parameters of each element at every time point of the year. The time-varying elements in the circuit included the substation voltage source, the PV array output, and the aggregated load. For the time-series analyses, the PV inverter was set to operate in autonomous Volt-VAR mode following a slightly modified version of the

Category B default settings [7] that allowed for maximum VAR injection and absorption at 0.95 and 1.05 p.u. voltage, respectively, as opposed to 0.92 and 1.08 p.u. This mode was selected to enable the inverter PF to vary over time (as a function of grid voltage and PV array power).

B. *Protection System Impact Metrics*

Two protection system impact metrics were selected to compare the results from the static and time-series fault studies: *desensitization* and *interrupt capability change*, both of which are measured in amps and are commonly evaluated in PV HCA. It was assumed that the protection devices were perfectly coordinated to detect and isolate faults before the PV system was installed. Therefore, the "PV Off" case represented the baseline fault current magnitude, $|I_{F_{Baseline}}|$. Both metrics were tracked for each of the two protective devices in Fig. 5.

Desensitization refers to the degree to which a protective device is less able to detect a fault. This metric is associated with the "minimum pick-up" current setting of a protective device, which specifies the current magnitude threshold that triggers the device. In other words, the device will not act if it senses currents below this threshold. Generally, distribution protection devices and set so that they will be able to detect and trip for a fault at the end of the feeder. When PV systems inject current during a fault, the fault current seen by a protective device may be reduced, meaning the device has become at least partially *desensitized* to the fault, or completely *desensitized* if the fault current is reduced below its minimum pick-up setting. For this work, $I_{Desensitization}$ is defined in (9) as:

$$I_{Desensitization} = min(|I_F|) - |I_{F_{Baseline}}| \quad (9)$$

On the other hand, current injections from PV systems can also increase the fault current seen by protective devices. The *interrupt capability* metric is associated with the physical device parameters that determine the largest current magnitude it can safely and reliably *interrupt*. If the fault current exceeds this threshold, a different protective device may respond instead and disconnect more customers than required, or the device will attempt to operate, risking device damage and/or failure. For this work, the *interrupt capability change* ($\Delta I_{Interrupt}$) is defined in (10) as:

$$\Delta I_{Interrupt} = \max(|I_F|) - |I_{F_{Baseline}}| \quad (10)$$

Since the PV system in Fig. 5 has a grid-following inverter, it injects balanced currents across all three phases [19]. Therefore, to simplify the analyses, the protection metrics are reported for one of the phase elements (Phase A).

V. Results

A. *Static Fault Analysis*

First, the static fault studies were conducted on the test circuit from Fig. 5 to determine the baseline fault current, $|I_{F_{Baseline}}|$, in the circuit (i.e., without any PV current injections). For this case, the fault current in the circuit was 1,837 A; since the relay and recloser are in series with one another and the PV system was off, the fault current was approximately the same for both devices aside from some losses. This result is represented as the horizontal dotted line "PV off" in Fig. 6.

The next test case represented the typical PV parameters used for evaluating protection impacts in HCA, in which the PV system is operating at full rated capacity (Irradiance = 1.0 kW/m^2) and unity PF. The results of each device for this case are represented by the intersection to the vertical dashed line "PV on (HCA)" in Fig. 6. In this case, the PV system injected 751.8 A of fault current in phase with the voltage at the node between the relay and recloser. For the plots on the right, note that the PV system had a DC/AC ratio of 1.3, so the inverter was operating at full capacity for any irradiance above 0.77 kW/m^2. Compared to the baseline scenario, less fault current was supplied from the substation, so the relay fault current was reduced to 1,619 A, or *desensitized* by 218 A (13.47%). The PV fault contribution also led to an increase in fault voltage compared to the baseline scenario, which increased the fault current through the recloser to 1,917 A, resulting in a $\Delta I_{Interrupt}$ of 80 A (4.17%). For context, the EPRI DRIVE tool for streamlined PV HCA [22] uses a default value of 10% to flag deviations in fault currents caused by PV injections.

In addition to the "PV off" and "PV on (HCA)" cases, static fault studies were conducted for a range of PV inverter PF conditions (left column plots in Fig. 6.) and irradiance levels (right column plots in Fig. 6.). Unlike the results in Fig. 2-Fig. 4, the inverter PCC voltage (bottom plots in Fig. 6) was dependent on the fault resistance and location—not directly controlled. These additional fault studies were intended to highlight just a portion of the potential impacts to relay and recloser fault currents, since the PV inverter can operate at essentially any combination of irradiance and PF.

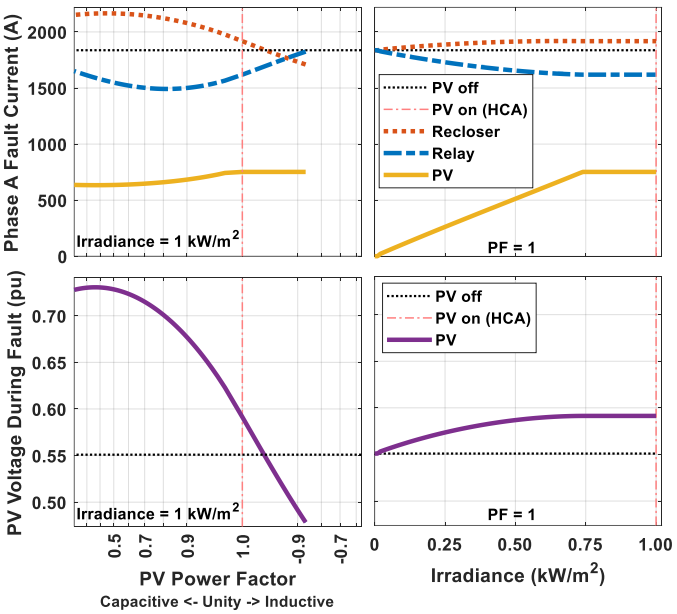

Fig. 6. Static fault study results depicting the impacts of time-varying PV parameters. The "PV on (HCA)" line highlights the conditions used for HCA, where PF=1 and Irradiance=1 kW/m^2 and the intersections with this line represent the results for each device.

As seen in the top left plot of Fig. 6, there were some PF values that caused more relay desensitization than the "PV on (HCA)" case, some that caused less, and others that resulted in larger fault currents through the relay than through the recloser. Some test conditions resulted in fault voltages that would have

required momentary cessation (i.e., <0.50 p.u.) [7], but these data points were included to show what would have happened if the inverter kept injecting fault current. Large-scale PV inverters connected to the transmission system should now be able to ride through voltages as low as 0.10 p.u. [21], so if similar requirements are adopted for distribution system interconnections, the range of potential protection systems impacts would expand. This same plot also highlights that the PV fault current angle alone can impact protection devices, which is in line with previous discussions [6]; from unity PF to -0.87, the PV fault current magnitude was at its limit, yet the relay and recloser fault currents continued to change.

B. Time-Series Fault Analysis

The static fault results in Fig. 6 are useful in analyzing the complex relationships between PV parameters and fault currents in a given test circuit, but they do not provide practical bounds for the combinations of irradiance and PF conditions that a PV inverter may operate at. Since the PV inverter PF may be dependent on atmospheric conditions, grid conditions, or centralized control objectives, time-series analysis is required. In this work, the PV inverter was set to operate in autonomous Volt-VAR mode with VAR priority, meaning the PF would change with the grid voltage at the PV inverter terminals as well as with the input power to the PV array.

Overall, the time-series fault analysis was accomplished with a two-step approach. First, a quasi-static time-series (QSTS) simulation was conducted on the circuit with time steps of 15 minutes for every time point of the year (35,040 total time points), but without any faults applied. In QSTS simulations, the solution of one time point serves as the initial state for the next, so the entire year was simulated consecutively while PV parameters and grid state variables were recorded. Thus, the results from this simulation provided the pre-fault conditions for every time point of the year. Next, fault studies were conducted for each of these time points after manually adjusting the circuit corresponding to the pre-fault conditions at that time, while fault currents and voltages throughout the circuit were recorded.

Results from the initial QSTS simulation are presented in Fig. 7, which shows the cumulative distribution function (CDF) plots for PV PF and real power output after filtering out nighttime data points when the PV is off. As anticipated, the PV inverter only operated at its full power output for less than 25% of the daylight hours throughout the year. This figure also shows that the PV inverter operated with PFs as low as 0.2 (inductive) but did not operate at any capacitive PFs. While IEEE 1547 says that the minimum reactive power requirements of an inverter do not require it to be able to handle 0.2 PF, the hardware tests showed that the inverter had no problem operating even very close to a power factor of zero.

An example of the time-series fault study results is presented in Fig. 8, which shows two consecutive days from the analysis selected at random. The first day highlights the variability associated with distributed PV, where the possible fault current rises and falls throughout the day as clouds pass over the PV array. In contrast, the second day depicts clear sky conditions for which the PV is able to inject its maximum current for a significant portion of the daylight hours. However, the most consequential time points on both days were actually in the early mornings and late afternoons when PV fault current magnitude was relatively low (see the zoomed-in section of Fig. 8); during these time periods, the recloser was briefly desensitized and the relay fault current is increased—the opposite of the behavior over the remaining time periods of the day. In these cases, even though the PV fault current magnitude was low, the PF required by the Volt-VAR control at those times was fairly extreme and ended up having an impact on the protection devices.

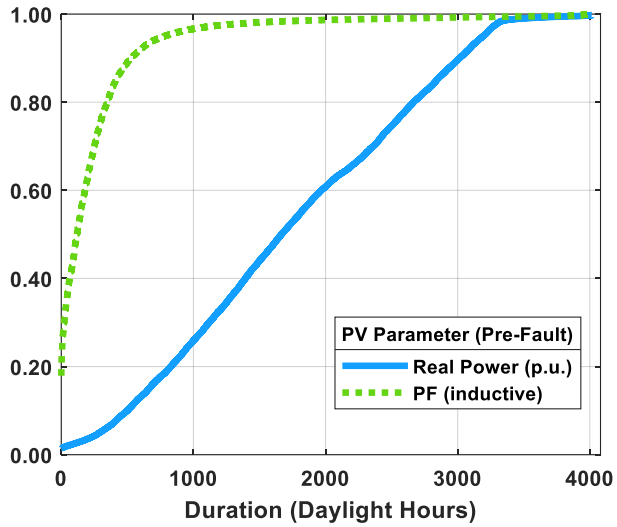

Fig. 7. Cumulative distribution plot of time-varying PV parameters from the pre-fault QSTS simulation.

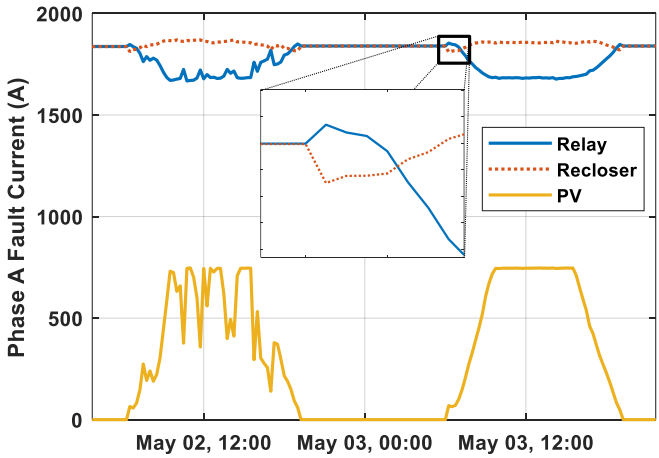

Fig. 8. Time-series fault study results for two random consecutive days.

The time-series fault behavior of the PV inverter for the rest of the year is summarized in Fig. 9. This figure shows all the combinations of fault current magnitudes and angles measured over the year, while the color of the pixel expresses the total duration of that combination (pixels in black represent combinations that did not occur). There were a wide variety of magnitude and angle combinations throughout the year but just a few current-limited combinations made up a significant portion of the total duration. Interestingly, *none* of the current-limited data points occurred at unity PF (i.e., with a fault current angle of 0°).

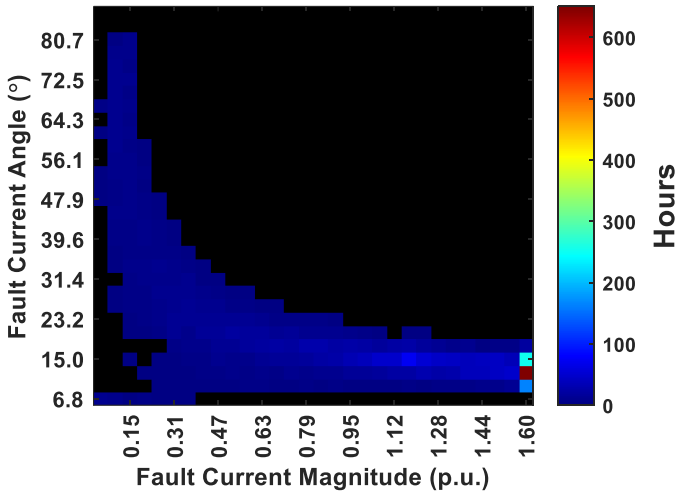

Fig. 9. Heatmap of the amount of time during the year that the PV inverter fault contributions would have been at that magnitude and angle.

C. *Static vs. Time-series Analysis*

The static and time-series fault study results for the relay and recloser fault currents are presented in Fig. 10, where the static results are represented by the horizontal lines and the time-series results are represented by CDF plots. Since the PV fault contribution generally had the opposite impact on the recloser compared to the relay, the recloser CDF is plotted in descending order to clarify the analyses. The dashed lines for the relay and recloser and black dotted "PV Off (Static)" line correspond to the "PV on (HCA)" and "PV off" results from Fig. 6, respectively. The results in Fig. 10 were used to evaluate the protection impact metrics from Section IV. B., which are summarized in Table I. For the relay desensitization impacts, the static fault study overestimated the time-series results by 27 A. However, this overestimation is likely acceptable since it is in the ballpark of the headroom that is typically applied when coordinating settings for protection devices. For impacts to interrupt capabilities, the static results detected no change, but the time-series study found an increase of 24 A. Although the magnitude of this discrepancy was not large in this case, it does indicate that the conventional methods may not sufficiently capture certain impacts.

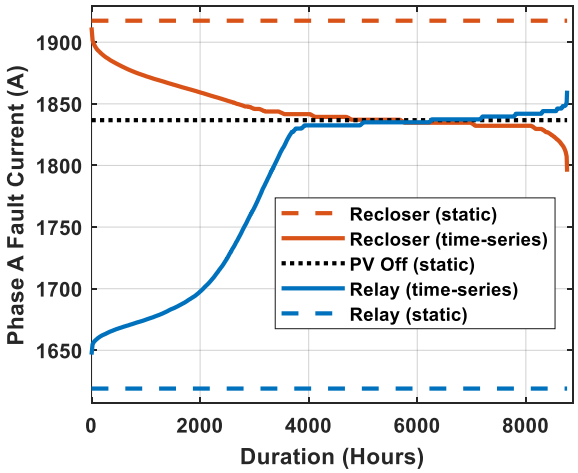

Fig. 10. Comparison of PV impacts on protection devices evaluated with static and time-series fault studies.

TABLE I. PROTECTION IMPACT METRIC COMPARISON

Device	$I_{Desensitization}$ (static)	$I_{Desensitization}$ (time-series)	$\Delta I_{Interrupt}$ (static)	$\Delta I_{Interrupt}$ (time-series)
Relay	218 A	191 A	0 A	24 A
Recloser	0 A	42 A	80 A	75 A

The takeaways for the recloser impacts were similar but for the opposite metrics. The static fault study slightly overestimated the change in interrupt capability (by just 5 A), but did not capture any of the desensitizing impacts of the PV fault contribution (42 A). Again, while the differences in magnitudes of the metrics may not be alarming in this case, it may be prudent to include additional scenarios to ensure static fault studies sufficiently capture all relevant protection impacts of distributed PV, particularly when grid-support functions or other advanced control objectives will be implemented.

VI. DISCUSSION

Although this work was not intended to cover all potential PV impacts on protection systems, there were some observations that could be applicable to the broader field. For instance, there was a significant difference between the actual current limit of the inverter tested in Section III. B. (1.625 p.u.) compared to typical values used to represent the current (~1.2 p.u.). So, if the information regarding a current limit of an inverter is missing from an inverter's technical datasheet, conventional assumptions may cause issues. Similarly, certain inverters limit their output current based on pre-fault operating conditions, yet the way in which the current limit is applied is also not required to be explained on datasheets.

The results in this work do indicate that time-series fault studies could provide additional value; the increase in the maximum fault current seen by the relay and the desensitization experienced by the recloser would not have been captured with the conventional approach. While the magnitude of those impacts was not particularly large, it is worth noting that this work was limited to a single test circuit focused on one of many possible inverter control functions (autonomous Volt-VAR). Although the settings for the Volt-VAR curve enabled the inverter to inject or absorb reactive power, the voltages at the inverter PCC over the year only ever required unity PF operation or reactive power absorption (see Fig. 7). According to Fig. 6, the maximum recloser fault current could have increased significantly above the unity PF case if the inverter had injected reactive power, while the minimum relay fault current could have been significantly reduced. For instance, if the distribution system operator had initiated a conservation voltage reduction (CVR) event, the same autonomous Volt-VAR settings would have attempted to boost the voltage back up by injecting reactive power. It is possible that if a fault occurred during a CVR event, the relay would have been desensitized more than the static case due to the angle of the PV fault current injection due to the reactive power injection before the fault. Alternatively, enabling the inverter to provide dynamic voltage support would have also resulted in PV reactive power injections during any fault. In other words, the fact that there was not a large difference between the static and time-series fault studies in this case is partly attributed to the simulation setup and selected controls.

As penetration levels of PV and other DERs increase, there will likely be more incentive to leverage advanced inverter capabilities through centralized/feeder-wide controls to improve grid conditions. If existing trends continue, inverters may be expected to ride through more extreme disturbances or even attempt to mitigate them. Thus, it is certainly conceivable that any given inverter could end up injecting its maximum fault current at much more extreme PFs than those shown in Fig. 9. So, while practical challenges of implementing full yearlong time-series fault studies may remain due to their relative complexity and computational burden, additional cases should be included in static fault studies to represent the most extreme expected combinations of fault current magnitudes and angles, with current limits of all simulated inverters set according to their actual hardware or software constraints.

VII. Conclusion

Assessing the impact of distributed PV systems and other DER installations on power system protection is becoming more crucial as penetration levels rise and as the utilization of advanced inverter capabilities increases. In this work, a time-series fault study framework was proposed and implemented. The results were compared to the conventional static fault study approach for evaluating common protection constraints of PV HCA. Both studies utilized a validated PV fault model that was developed by testing a commercial off-the-shelf inverter under a variety of irradiances, fault voltages, and control settings. While the conventional static approach captured certain metrics well, not all PV impacts from the time-series results were captured. Overall, conducting time-series fault studies may be prohibitively burdensome in many cases, but the results in this work indicate that the static approach can be improved by including additional scenarios to analyze, ensuring protection systems remain reliable in the presence of distributed PV with advanced inverter functions enabled.

Acknowledgment

Thank you to Michael Ropp and Shibani Ghosh for their review and suggestions on this work.

References

[1] S. Stanfield, Y. Zakai, and M. McKerley, "Key Decisions for Hosting Capacity Analysis," IREC, 2021.

[2] "IEEE Guide for Loading Mineral-Oil-Immersed Transformers and Step-Voltage Regulators," *IEEE Std C57.91-2011 (Revision of IEEE Std C57.91-1995),* pp. 1-123, 2012.

[3] *ANSI C84.1-2020 American National Standard For Electric Power Systems and Equipment - Voltage Ratings (60 Hz)*, ANSI, 2020.

[4] "IEEE Standard for Interconnection and Interoperability of Distributed Energy Resources with Associated Electric Power Systems Interfaces--Amendment 1: To Provide More Flexibility for Adoption of Abnormal Operating Performance Category III," *IEEE Std 1547a-2020 (Amendment to IEEE Std 1547-2018),* pp. 1-16, 2020, doi: 10.1109/IEEESTD.2020.9069495.

[5] A. K. Jain, K. Horowitz, F. Ding, K. S. Sedzro *et al.*, "Dynamic hosting capacity analysis for distributed photovoltaic resources—Framework and case study," *Applied Energy,* 2020.

[6] N. S. Gurule, J. A. Azzolini, R. Darbali-Zamora, and M. J. Reno, "Impact of Grid Support Functionality on PV Inverter Response to Faults," in *2021 IEEE 48th Photovoltaic Specialists Conference (PVSC)*, 20-25 June 2021 2021, pp. 1440-1447.

[7] *IEEE 1547 Standard for Interconnection and Interoperability of Distributed Energy Resources with Associated Electric Power Systems Interfaces*, IEEE, 2018.

[8] R. Darbali-Zamora, J. Johnson, N. S. Gurule, M. J. Reno, N. Ninad, and E. Apablaza-Arancibia, "Evaluation of Photovoltaic Inverters Under Balanced and Unbalanced Voltage Phase Angle Jump Conditions," in *2020 47th IEEE Photovoltaic Specialists Conference (PVSC)*, 15 June-21 Aug. 2020 2020, pp. 1562-1569.

[9] N. S. Gurule, J. Hernandez Alvidrez, M. J. Reno, and J. Flicker, "Multiple Inverter Microgrid Experimental Fault Testing," *49th IEEE Photovoltaic Specialists Conference (PVSC 49)*, 2022.

[10] K. Ardani, E. O'Shaughnessy, and P. Schwabe, "Coordinating Distributed Energy Resources for Grid Services: A Case Study of Pacific Gas and Electric," National Renewable Energy Laboratory, Golden, CO, 2018.

[11] H. Yazdanpanahi, Y. W. Li, and W. Xu, "A New Control Strategy to Mitigate the Impact of Inverter-Based DGs on Protection System," *IEEE Transactions on Smart Grid,* vol. 3, no. 3, pp. 1427-1436, 2012.

[12] R. A. Walling, R. Saint, R. C. Dugan, J. Burke, and L. A. Kojovic, "Summary of Distributed Resources Impact on Power Delivery Systems," *IEEE Transactions on Power Delivery,* vol. 23, no. 3, pp. 1636-1644, 2008.

[13] J. Seuss, M. J. Reno, R. J. Broderick, and S. Grijalva, "Determining the Impact of Steady-State PV Fault Current Injections on Distribution Protection," Sandia National Laboratories, SAND2016, 2016.

[14] Y. Tang, T. McDermott, and J. Homer, "Summary of electric distribution system analyses with a focus on DERs," in *2018 IEEE Power & Energy Society Innovative Smart Grid Technologies Conference (ISGT)*, pp. 1-5, 2018.

[15] G. Kou, L. Chen, P. VanSant, F. Velez-Cedeno, and Y. Liu, "Fault Characteristics of Distributed Solar Generation," *IEEE Trans. Power Deliv.,* vol. 35, no. 2, pp. 1062-1064, 2020.

[16] J. Hernandez-Alvidrez, A. Summers, N. Pragallapati, M. J. Reno *et al.*, "PV-Inverter Dynamic Model Validation and Comparison Under Fault Scenarios Using a Power Hardware-in-the-Loop Testbed," in *IEEE 7th World Conference on Photovoltaic Energy Conversion (WCPEC)*, 2018.

[17] Y. N. Velaga, R. Jain, and J. Sawant, "Modeling Distributed Energy Resources for Analyzing Distribution Systems with High Renewable Penetration," presented at the IEEE Rural Electric Power Conference, United States, 2022.

[18] S. Gonzalez, N. Gurule, M. J. Reno, and J. Johnson, "Fault Current Experimental Results of Photovoltaic Inverters Operating with Grid-Support Functionality," in *IEEE 7th World Conference on Photovoltaic Energy Conversion (WCPEC)*, 2018.

[19] M. J. Reno, S. Brahma, A. Bidram, and M. E. Ropp, "Influence of Inverter-Based Resources on Microgrid Protection: Part 1: Microgrids in Radial Distribution Systems," *IEEE Power and Energy Magazine,* vol. 19, no. 3, pp. 36-46, 2021.

[20] EPRI. "Open Distribution System Simulator (OpenDSS)." http://sourceforge.net/projects/electricdss/.

[21] *IEEE Standard for Interconnection and Interoperability of Inverter-Based Resources (IBRs) Interconnecting with Associated Transmission Electric Power Systems*, IEEE Std 2800™-2022, IEEE, 2022.

[22] M. Rylander, J. Smith, and W. Sunderman, "Streamlined Method for Determining Distribution System Hosting Capacity," *IEEE Trans. Ind. Appl.,* vol. 52, no. 1, pp. 105-111, 2016.